Correlation between self-diffusion in Si and the migration mechanisms of vacancies and self-interstitials: An atomistic study

M. Posselt,[1,*] F. Gao,[2] and H. Bracht[3]

[1]*Forschungszentrum Dresden-Rossendorf, Institute of Ion Beam Physics and Materials Research, P.O. Box 510119, D-01314 Dresden, Germany*

[2]*Pacific Northwest National Laboratory, Fundamental Science Directorate, P.O. Box 999, Richland, Washington 99352, USA*

[3]*Institut für Materialphysik, University of Münster, Wilhelm-Klemm Strasse 10, D-48149 Münster, Germany*

(Received 31 March 2008; published 21 July 2008)

The migration of point defects in silicon and the corresponding atomic mobility are investigated by comprehensive classical molecular-dynamics simulations using the Stillinger-Weber potential and the Tersoff potential. In contrast to most of the previous studies both the point defect diffusivity and the self-diffusion coefficient per defect are calculated separately so that the diffusion-correlation factor can be determined. Simulations with both the Stillinger-Weber and the Tersoff potential show that vacancy migration is characterized by the transformation of the tetrahedral vacancy to the split vacancy and vice versa and the diffusion-correlation factor f_V is about 0.5. This value was also derived by the statistical diffusion theory under the assumption of the same migration mechanism. The mechanisms of self-interstitial migration are more complex. The detailed study, including a visual analysis and investigations with the nudged elastic band method, reveals a variety of transformations between different self-interstitial configurations. Molecular-dynamics simulations using the Stillinger-Weber potential show that the self-interstitial migration is dominated by a dumbbell mechanism, whereas in the case of the Tersoff potential the interstitialcy mechanism prevails. The corresponding values of the correlation factor f_I are different, namely, 0.59 and 0.69 for the dumbbell and the interstitialcy mechanisms, respectively. The latter value is nearly equal to that obtained by the statistical theory which assumes the interstitialcy mechanism. Recent analysis of experimental results demonstrated that in the framework of state-of-the-art diffusion and reaction models the best interpretation of point defect data can be given by assuming $f_I \approx 0.6$. The comparison with the present atomistic study leads to the conclusion that the self-interstitial migration in Si should be governed by a dumbbell mechanism.

DOI: 10.1103/PhysRevB.78.035208 PACS number(s): 61.72.Bb, 85.40.Ry, 61.80.Az

I. INTRODUCTION

Under intrinsic conditions self-diffusion in silicon may be caused by vacancies (V), self-interstitials (I), mobile vacancy and self-interstitial clusters, as well as by the direct exchange of atoms. Experimental and theoretical investigations showed that the latter mechanism[1] does not play an important role and can be therefore neglected.[2–6] The contribution of a certain mobile defect of a given charge state to self-diffusion is proportional to the product of the defect concentration per silicon atom and its diffusivity. Thus the self-diffusion coefficient D_{sd} may be determined by

$$D_{\mathrm{sd}} = \sum_k f_{V^k} C_{V^k} D_{V^k} + \sum_l f_{I^l} C_{I^l} D_{I^l} + \sum_m f_{V_2^m} C_{V_2^m} D_{V_2^m} + \sum_n f_{I_2^n} C_{I_2^n} D_{I_2^n} + \cdots . \quad (1)$$

Here the contribution of mobile defect clusters that contain more than two vacancies or self-interstitials is not considered explicitly. The sums are over all relevant charge states of the defect. C_{V^i}, D_{V^i}, C_{I^i}, D_{I^i}, $C_{V_2^i}$, $D_{V_2^i}$, $C_{I_2^i}$, and $D_{I_2^i}$ denote the relative concentrations and the diffusivities of vacancies, self-interstitials, divacancies, and di-interstitials, respectively. The quantities f_{V^i}, f_{I^i}, $f_{V_2^i}$, and $f_{I_2^i}$ are called diffusion-correlation factors since they describe the correlation between the migration of the respective defect and the mobility of the silicon atoms. Depending on the charge state, different configurations of vacancies, self-interstitials, and defect clusters may exist. Furthermore, in a given charge state these defects may have one stable and several metastable configurations. During migration vacancies or self-interstitials may be transformed from one state to another. It is very difficult to determine all contributions to D_{sd} separately. Most authors consider self-diffusion in thermal equilibrium.[2–4,7] In this case self-diffusion is dominated by the contribution of vacancies and self-interstitials. This is because the formation energy of the defect clusters is relatively high (cf. Ref. 8) and, consequently, their equilibrium concentration is very small compared to that of vacancies and self-interstitials. Using silicon isotope heterostructures the self-diffusion coefficient in thermal equilibrium was accurately determined over 7 orders of magnitude.[3] It was found that the temperature dependence of D_{sd} can be well described by a single Arrhenius term with an activation energy of 4.75 eV. Furthermore, it is generally supposed that the diffusion-correlation factors of all charge states of the vacancy and the self-interstitial are equal.[9,10] Applying the assumptions mentioned above the self-diffusion coefficient D_{sd} is given by

$$D_{\mathrm{sd}} = f_V P_V + f_I P_I, \quad P_V = \sum_l C_{V^l} D_{V^l}, \quad P_I = \sum_l C_{I^l} D_{I^l}. \quad (2)$$

The quantities P_V and P_I are called transport capacities and are defined as the sum over the products of the (relative)

 ©2008 The American Physical Society

equilibrium concentration and the diffusivity in the corresponding charge state. P_V and P_I were determined separately by metal diffusion experiments[2,4,11–13] as well as by dopant diffusion studies in isotopically enriched silicon structures under oxidation and nitridation conditions.[5,14] P_V and P_I could also be described by single Arrhenius terms. However, different authors obtained different values for the activation energies and the pre-exponential factors. In particular the values for P_V are still controversial. The situation is complicated by the fact that the diffusion-correlation factors f_V and f_I are also not very well known so that a direct comparison with the self-diffusion coefficient via Eq. (2) is nontrivial. Frequently[2–4,7] $f_V=0.5$ and $f_I=0.73$ are used. These values were determined within the framework of the statistical diffusion theory[15,16] by explicitly assuming the simple vacancy mechanism and the interstitialcy mechanism for self-diffusion by vacancies and self-interstitials, respectively. However, the investigations of Voronkov and Falster[17] showed that the value of f_I must be about 0.6 in order to obtain an activation energy of 4.5 eV for P_V, which is most consistent with experimental data from wafer processing. This result was obtained using D_{sd} from Ref. 3, P_I from metal diffusion experiments,[2,4] as well as by supposing $f_V=0.5$. Recently, Bracht *et al.*[10] analyzed experimental data which were obtained from their studies on simultaneous self-diffusion and dopant diffusion in isotope heterostructures. In these investigations, D_{sd} from Ref. 3 and P_I from Ref. 2 were used. Furthermore, it was assumed that the diffusivities of charged vacancies and self-interstitials are equal to the diffusivity of the corresponding neutral defect, and f_V was set to 0.5. The analysis showed that the value of f_I must be about 0.56 to get an activation energy of 4.6 eV for P_V. This value is consistent with the fact that the activation energy for Sb diffusion in Si is 4.1 eV. Since Sb diffuses by the vacancy mechanism, this activation energy must be smaller than that for P_V due to attractive electrostatic and elastic interactions between Sb and V.[10,18] This attraction does not exist in the case of Si self-diffusion by vacancies.

The previous discussion shows that the accurate determination of separate contributions of vacancies and self-interstitial to D_{sd} is hindered not only by the partially insufficient knowledge of the respective transport capacities but also by the lack of precise values for the diffusion-correlation factors f_V and f_I. The present work deals with an atomistic study on the correlation between self-diffusion and the migration mechanisms of vacancies and self-interstitials aiming to a better understanding of the diffusion-correlation factors. For this purpose the self-diffusion coefficient per point defect as well as the point defect diffusivity is calculated by classical molecular-dynamics (MD) simulations. The ratio of both quantities yields the corresponding diffusion-correlation factor. In this manner f_V and f_I can be determined without any assumptions about the atomic migration mechanisms, in contrast to the statistical diffusion theory,[15,16] where these mechanisms must be explicitly assumed. In the framework of present fundamental investigations on the diffusion-correlation factor, only neutral vacancies and self-interstitials can be considered, i.e., Eq. (2) is reduced to

$$D_{\mathrm{sd}} = f_V C_V D_V + f_I C_I D_I, \tag{3}$$

where C_V, D_V and C_I, D_I are the (relative) equilibrium concentration and the diffusivity of the neutral vacancies and self-interstitials, respectively. The migration mechanisms of the point defects may depend on the interatomic potential used in MD simulations. In the present work both the Stillinger-Weber (SW) potential[19] and the Tersoff potential[20] are considered. The atomic mechanisms of V and I migrations are studied in detail, including a visual analysis and investigations with the nudged elastic band method. The results on point defect migration obtained in the present work are compared with literature data which were obtained by MD simulations using classical interatomic potentials, tight-binding models, and the density-functional theory. A detailed comparison with the corresponding data extracted from experimental results is not performed since this would go beyond the scope of the present work that is focused on the fundamental study of the correlation between self-diffusion and the main migration mechanisms of V and I.

II. SIMULATION METHOD

Present investigations employ MD simulations with classical interatomic potentials. This method is very well suited for the study of migration processes under relatively realistic conditions, since it allows the consideration of several thousands of atoms and/or a time scale up to 1 μs. This is hardly possible if tight-binding MD or even MD simulations based on the density-functional theory would be used because they are much more computationally intensive than classical MD simulations. The SW potential[19] and the Tersoff 3 (T3) potential[20] are the most commonly used interatomic potentials for silicon, and their features have been extensively studied. It will be shown in Sec. III that in general they yield different configurations, formation energies, migration mechanisms, and migration energies for the vacancy and the self-interstitial. Therefore, a comparative study of both interatomic potentials is very useful for a better understanding of the diffusion-correlation factor. Throughout this work in all calculations with the SW potential a slightly changed value of the energy parameter ε ($\varepsilon=1.07\varepsilon_{\mathrm{original}}$) is used. This modification yields the correct cohesive energy of silicon.[21]

The simulation cell is a cubelike rectangular parallelepiped with x, y, and z directions parallel to the [−110], [−1−12], and [111] axes, respectively. Three-dimensional periodic boundary conditions are used. The cell consists of 1008 ± 1 atoms if a single self-interstitial or a single vacancy is investigated, respectively.

The formation energy and the formation volume of vacancy and self-interstitial configurations are calculated in the following manner. Starting with the ideal defect configuration found by symmetry considerations or with the defect configuration obtained by heating up the simulation cell with the ideal configuration to a certain temperature, the relaxed defect structure at 0 K is determined by rapid quenching using MD simulations. The relaxation is performed for several similar but slightly different values of the lattice constant. For the final configurations the quantities

$$E^{V/I} = E^{V/I}_{n\mp1} - \frac{n \mp 1}{n} E^0_n \tag{4}$$

and

$$\Omega^{V/I} = \Omega^{V/I}_{n\mp1} - \frac{n \mp 1}{n} \Omega^0_n \tag{5}$$

are determined, where E^0_n and Ω^0_n denote the cohesive energy and the volume of a simulation cell containing a perfect crystal with n atoms at 0 K. $E^{V/I}_{n\mp1}$ and $\Omega^{V/I}_{n\mp1}$ are the cohesive energy and the volume of the system with a relaxed defect configuration. In $E^{V/I}_{n\mp1}$ and $\Omega^{V/I}_{n\mp1}$, as well as in Eqs. (4) and (5), the minus and the plus signs are related to the vacancy and the self-interstitial, respectively. The lowest value of $E^{V/I}$ found during the variation of the lattice constant defines the defect formation energy $E^{V/I}_f$ and the corresponding value of $\Omega^{V/I}$ is the defect formation volume $\Omega^{V/I}_f$.

The migration of a single vacancy or a single self-interstitial is considered within the framework of the isobaric-isothermal ensemble (N,P,T with $P=0$). The simulation starts with a simulation cell at 0 K, containing a vacancy or a self-interstitial configuration with low formation energy. Then, the cell is coupled to a Berendsen barostat to maintain the zero pressure boundary condition, and the atoms of the outermost layer of the cell are connected to a Berendsen thermostat.[22] After heating up the system to the desired temperature, the migration of the point defect and of the Si atoms is followed for different periods. The lower the temperature, the longer the MD simulation is. In the present work the simulation time and the temperature vary from 5 to 1200 ns and from 1600 to 800 K, respectively. The atomic mobility due to the presence of a single vacancy or a single self-interstitial is characterized by the time dependence of the sum of the squared displacements ssd_a of all atoms,

$$\mathrm{ssd}_a(t) = \sum_{i=1}^{N} [\mathbf{r}_i(t) - \mathbf{r}_i(0)]^2, \tag{6}$$

where $\mathbf{r}_i(0)$ is the position of atom i at the beginning of the migration simulation and $\mathbf{r}_i(t)$ is the position at time t. N denotes the total number of atoms in the simulation cell. The self-diffusion coefficient per vacancy or self-interstitial (D_s) is obtained by fitting $\mathrm{ssd}_a(t)$ to a linear expression and by employing the Einstein relation,[23,24]

$$\mathrm{ssd}_a(t) = \mathrm{const} + 6D_s t. \tag{7}$$

The constant corresponds to the sum of the squared displacements of the atoms in the perfect crystal at a given temperature.

The diffusivity D_d of a point defect is calculated in the following manner. During the simulation, the point defect position is monitored by analyzing the Wigner-Seitz cells of the perfect lattice. A Wigner-Seitz cell that contains two atoms is identified with the location of the self-interstitial and an empty cell corresponds to the location of the vacancy. Based on the Wigner-Seitz cell analysis, the trajectory of the point defect is determined.[24,25] In order to obtain the diffusivity of the point defect, its trajectory is decomposed into time segments,[24–26] and for each segment m the squared displacement sd_d of the position $\mathbf{R}(t)$ of the point defect is calculated: $\mathrm{sd}_d(m) = [\mathbf{R}(t_m) - \mathbf{R}(t_{m-1})]^2$, $t_m = t_{m-1} + \Delta t$. Applying the Einstein relation and averaging over all segments n_s lead to the defect diffusion coefficient,

$$D_d = \frac{1}{n_s} \sum_{m=1}^{n_s} \frac{\mathrm{sd}_d(m)}{6\Delta t}. \tag{8}$$

Within certain limits the number (or the size) of the time intervals can be chosen arbitrarily.[24–26] Therefore, a further averaging can be performed over all possible decompositions. In this manner, an improvement of the statistical accuracy of the result is possible.

The ratio of the self-diffusion coefficient per point defect and the point defect diffusivity yields the diffusion-correlation factor since

$$D_s = f D_d. \tag{9}$$

This relation can be derived from Eq. (3), for example, if the migration of a single vacancy is simulated ($C_I=0$), one obtains

$$\frac{D_{\mathrm{sd}}}{C_V} = D^V_s = f_V D_V. \tag{10}$$

In addition to the calculations of diffusion coefficients, the atomic mechanisms of the migration of vacancies and self-interstitials are investigated in detail. For this purpose, the defect trajectories and the atomic rearrangements during the defect migration are analyzed using visualization tools. Furthermore, the nudged elastic band method[27,28] is applied to investigate the potential energies along certain migration paths at $T=0$ K.

III. RESULTS AND DISCUSSION

A. Structure and energetics of point defects

The data for the formation energy and formation volume of point defect configurations are summarized in Table I. Both for the SW and the T3 potential the structure and energetics of vacancies and self-interstitial configurations were already investigated by several authors[21,29–34] whereas only very few data on the formation volume are available. In the case of the SW potential the tetrahedral vacancy and the extended ⟨110⟩ dumbbell are the most stable vacancy and self-interstitial configurations, respectively. The strong inward relaxation of the atoms around the vacancy leads to a negative formation volume. The use of the T3 potential yields the split vacancy and the tetrahedral interstitial as most stable vacancy and self-interstitial defects, respectively. The atoms around the tetrahedral vacancy show a strong outward relaxation, whereas an inward relaxation is observed around the split vacancy. The values for the formation energy given in Table I as well as the results on the relaxation of the atoms around the point defects are consistent with previous data obtained by the SW and the T3 potentials.[21,29–34] A comparison with results obtained by other theoretical methods such as tight-binding methods and density-functional theory is beyond the scope of the present work.

TABLE I. Formation energy and formation volume of different vacancy and self-interstitial configurations. Note that in a perfect crystal the volume per atom is 20.0 Å^3. In the case of the SW potential the split vacancy and the hexagonal interstitial are not stable. For the T3 potential two different extended ⟨110⟩ dumbbell configurations are found, and the data given for the hexagonal interstitial concern the so-called bond centered configuration (Refs. 29 and 30).

	SW potential		T3 potential	
Defect configuration	E_f (eV)	Ω_f (Å^3)	E_f (eV)	Ω_f (Å^3)
Tetrahedral vacancy	2.82	−13.4	3.70	31.2
Split-vacancy			3.49	−2.27
Tetrahedral interstitial	5.25	24.7	3.45	13.5
Hexagonal interstitial			4.07	2.27
⟨110⟩ dumbbell	4.71	13.5	4.40	2.27
Extended ⟨110⟩ dumbbell	3.91	2.40	3.83, 4.73	−8.82, 2.27
⟨100⟩ dumbbell	5.62	2.40	4.70	2.27

B. Point defect migration and diffusion-correlation factors

1. Vacancy

Figures 1(a) and 1(b) show the diffusivity of the vacancy D_V and the self-diffusion coefficient per vacancy D_s^V in an Arrhenius plot. In the temperature range considered, D_V and D_s^V depend linearly on the inverse temperature. The T3 potential yields lower values for D_V and D_s^V than the SW potential. The effective migration barrier is very similar to that found for the SW potential (Table II). For both potentials the visual analysis of vacancy migration shows a simple mechanism: One of the four atoms that surround the tetrahedral vacancy moves toward and then into the vacant lattice site leaving behind a vacancy on its initial site. The split vacancy is only a transition state. Such a mechanism was also assumed by Compaan and Haven[15] in order to describe self-diffusion via the simple vacancy mechanism. Therefore the diffusion-correlation factor obtained by classical MD simulations is nearly identical to the value derived by the statistical diffusion theory (f_V=0.5).[15] The small deviations are due to the statistical errors which occur in the calculation of the diffusion coefficients (Table II). For comparison Table III shows the results of previous MD simulations on vacancy migration. The data obtained using the SW potential are very similar to those calculated in this work. MD simulations based on the tight-binding model and on density-functional theory yield lower effective migration barriers and the diffusivities are mostly higher. However, the mechanism of vacancy migration observed in these investigations is very similar to that found in the present work. It should be noted that in most of the previous MD simulations, either the vacancy diffusivity D_V or the self-diffusion coefficient per vacancy D_s^V was determined so that a calculation of the diffusion-correlation factor was not possible. The only exception is the comprehensive work of Sahli[40] where MD simulations based on the density-functional theory were performed. They obtained a value for the diffusion-correlation factor f_V which is consistent with that obtained in the present work.

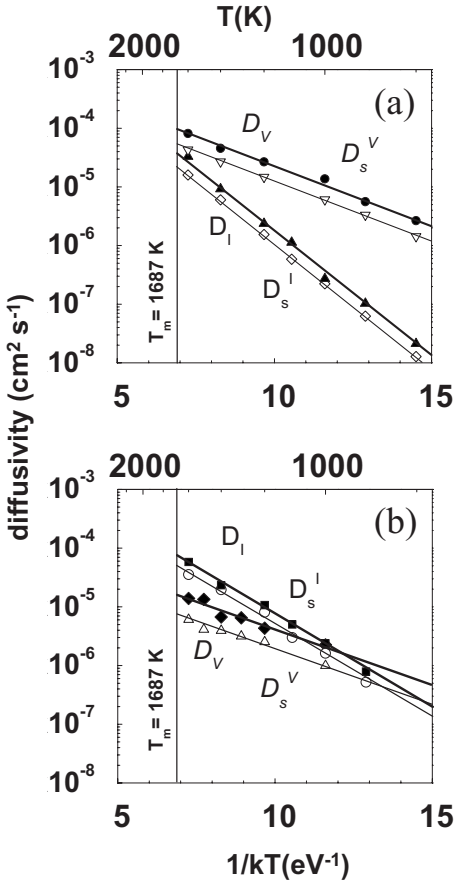

FIG. 1. Defect diffusivities D_I and D_V (filled symbols and thick lines) and self-diffusion coefficients per defects D_s^I and D_s^V (open symbols and thin lines) obtained by MD simulations using (a) the Stillinger-Weber potential (Ref. 19) and (b) the Tersoff potential (Ref. 20). Meaning of the different symbols in figure (a): filled triangles—D_I; filled circles—D_V; open diamonds—D_s^I; and open upside down triangles—D_s^V. Meaning of the symbols in figure (b): filled squares—D_I; filled diamonds—D_V; open circles—D_s^I; and open triangles—D_s^V. The lines are drawn as a guide for the eyes. The values for the effective migration barriers and the preexponential factors are given in Table II. T_m denotes the melting temperature of silicon.

In the case of the SW potential the nudged elastic band method was applied to determine the potential energy along the migration path at T=0 K (Fig. 2). The tetrahedral vacancy is the initial and the final configuration and the saddle point corresponds to the split vacancy. The barrier is slightly higher than the effective migration barrier determined by MD simulations. Obviously, the vibrational motion of the lattice atoms causes an effective decrease in the barrier. It should be emphasized that MD simulations yield the Gibbs free energy of migration that includes entropy contributions, whereas the nudged elastic band method gives solely the energy barrier at T=0 K.

The fact that the split vacancy is the most stable vacancy configuration of the T3 potential at T=0 K seems to contradict the results of MD simulations for the T3 potential, in

TABLE II. Values of the pre-exponential factor and the effective migration barrier for the quantities D_V, D_s^V, D_I, and D_s^I shown in the Arrhenius plots in Figs. 1(a) and 1(b), as well as the values for the diffusion-correlation factors f_V and f_I. The statistical errors of the data for E_m, D_0, and f are about 2%, 5%, and 10%, respectively, with the exception of the case of the vacancy for the T3 potential where the statistical error is about a factor of 2 higher.

	Vacancy			Self-interstitial		
	D_0 ($cm^2\ s^{-1}$)	E_m (eV)	f_V	D_0 ($cm^2\ s^{-1}$)	E_m (eV)	f_I
			SW potential			
$D_{V/I}$	2.51×10^{-3}	0.47	0.53	3.31×10^{-2}	0.98	0.59
$D_s^{V/I}$	1.33×10^{-3}	0.47		1.95×10^{-2}	0.98	
			T3 potential			
$D_{V/I}$	3.16×10^{-4}	0.43	0.46	1.12×10^{-2}	0.73	0.69
$D_s^{V/I}$	1.46×10^{-4}	0.43		7.73×10^{-3}	0.73	

particular, the finding that the vacancy migration mechanism is very similar to that obtained for the SW potential where the split vacancy is only a transition state and the tetrahedral vacancy is most stable. The resolution of this apparent discrepancy will be the subject of a forthcoming paper. Here it should be only mentioned that in the case of the T3 potential the effective migration barrier of the vacancy is indeed constant in the temperature range studied in the present work but it may change (increase) at lower temperatures.[30]

2. Self-interstitial

The diffusivity of the self-interstitial D_I and the self-diffusion coefficient per self-interstitial D_s^I are depicted in Figs. 1(a) and 1(b). In the temperature range investigated by MD simulations the temperature dependence of these quantities can be described by Arrhenius relations, both for the SW and the T3 potentials. The SW potential gives lower values for D_I and D_s^I as well as a higher effective migration barrier than the T3 potential (Table II). The results of previous MD simulations[23,33,35–39] are listed in Table III. With the exception of the data of Kakimoto *et al.*[37] the results obtained by using the SW potential and the T3 potential are rather similar to the data given in Table II. Tight-binding MD simulations yield a higher migration barrier, whereas MD simulations based on the density-functional theory give a

TABLE III. Results of previous MD simulations on the migration of vacancies and self-interstitials: (i) MD simulations using classical interatomic potentials (SW and T3 potential), (ii) tight-binding MD, and (iii) MD simulations based on the density-functional theory. The denotations of the quantities are the same as in Table II.

		Vacancy		Self-interstitial	
		D_0 ($cm^2\ s^{-1}$)	E_m (eV)	D_0 ($cm^2\ s^{-1}$)	E_m (eV)
			SW potential		
Ref. 35	$D_{V/I}$			3.9×10^{-2}	0.89
Ref. 23	$D_s^{V/I}$	1.5×10^{-3}	0.43	1.6×10^{-2}	0.9
Ref. 36	$D_s^{V/I}$	1.7×10^{-3}	0.46	1.76×10^{-2}	0.94
Ref. 37	$D_s^{V/I}$		0.4		0.78
			T3 potential		
Ref. 33	$D_s^{V/I}$			3.04×10^{-2}	0.77
			Tight-binding theory		
Ref. 38	$D_s^{V/I}$	1.8×10^{-4}	0.1	1.58×10^{-1}	1.37
Ref. 39	$D_{V/I}$	4.1×10^{-4}	0.13	1.65×10^{-1}	1.2
			Density-functional theory		
Refs. 40 and 41	$D_{V/I}$	5.7×10^{-4}	0.17	5.2×10^{-3}	0.45
Refs. 40 and 41	$f_{V/I}$	0.54		0.75	

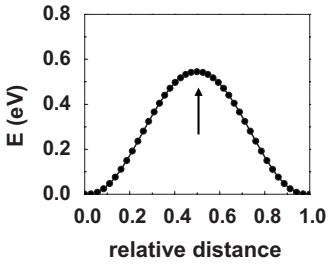

FIG. 2. Potential energy along the migration path from one tetrahedral vacancy to another, determined by the nudged elastic band method using the Stillinger-Weber potential (Ref. 19). The line is drawn as a guide for the eyes. The arrow marks the saddle point (split vacancy).

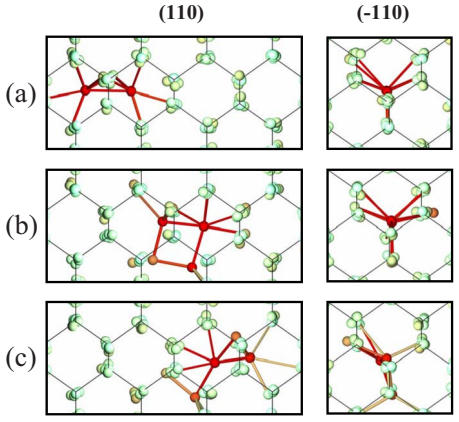

FIG. 3. (Color online) Snapshots from a movie with typical results of MD simulations of self-interstitial migration using the Stillinger-Weber potential (Ref. 19). The figures illustrate the first migration path which is characterized by the transformation from (a) the ⟨110⟩ dumbbell to (b) the extended ⟨110⟩ dumbbell and (c) vice versa. The views onto the (110) and (−110) planes demonstrate that the self-interstitial configuration moves within a {110} plane and into a ⟨110⟩ direction. The colored spheres show the atoms in the real lattice. The color is a measure for the deviation of atomic positions from the ideal lattice sites. Red and light green colors mean large and small deviations, respectively. In gray scale the red and light green colors correspond to dark and light gray, respectively. The light gray lines depict the bonds in the ideal lattice. Bonds between atoms in the real lattice are not shown, with the exception of those between the atoms belonging to the self-interstitial configuration and their neighbors. The color of these bonds varies with the colors of the two atoms forming the bond.

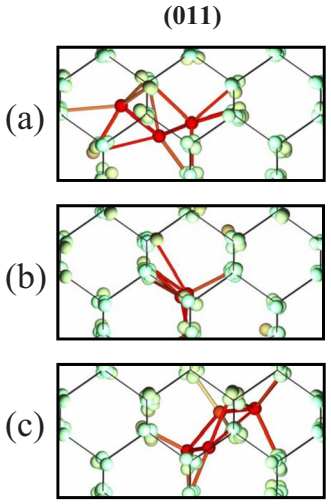

FIG. 4. (Color online) Snapshots from a movie with characteristic results of MD simulations of self-interstitial migration using the Stillinger-Weber potential (Ref. 19). The figures show the second migration path which is characterized by the transformation from (a) the extended ⟨110⟩ dumbbell to (b) the ⟨110⟩ dumbbell and (c) vice versa. In contrast to Fig. 3 the migration does not occur within a {110} plane but it includes a change into an equivalent {110} plane. The extended ⟨110⟩ dumbbells are not in the plane of (a) and (c). (b) shows a view perpendicular to the ⟨110⟩ dumbbell; therefore one atom of the dumbbell is hidden by the other. For details of the presentation, see Fig. 3.

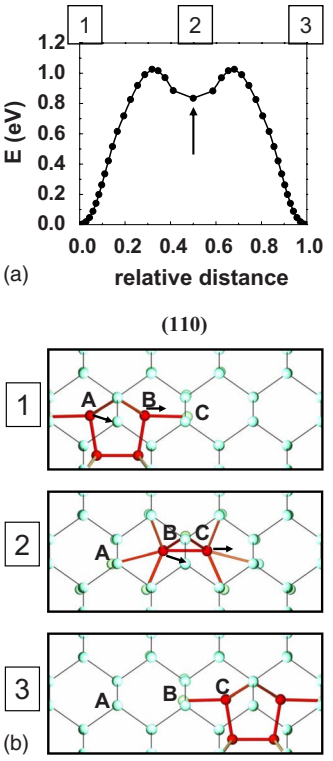

FIG. 5. (Color online) Investigation of the first migration path of the self-interstitial (cf. Fig. 3) using the nudged elastic band method: (a) depicts the potential energy along the path, from the extended ⟨110⟩ dumbbell to the ⟨110⟩ dumbbell (arrow) and vice versa, whereas (b) shows schematically the exchange of atoms during the transformation between these configurations.

lower value than that obtained in the present work.

The detailed analysis of the trajectories of the self-interstitial reveals that the use of the SW potential and the T3 potential leads to different migration mechanisms. In the case of the SW potential two migration paths dominate. The first path is characterized by the transformation from the extended ⟨110⟩ dumbbell to the ⟨110⟩ dumbbell and vice versa, which takes place in a {110} plane. Snapshots from a movie showing typical results of MD simulations are depicted in Fig. 3. The figure illustrates that the motion of the self-interstitial configuration occurs not only in a {110} plane but is also directed into a ⟨110⟩ direction. The atoms belonging to the self-interstitial change continuously and in such a manner, that the atomic mobility given by D_s^I is smaller than the mobility D_I of the self-interstitial itself. Likewise, the second path consists of a transformation from the extended ⟨110⟩ dumbbell to the ⟨110⟩ dumbbell and vice versa. However, this process does not take place within a {110} plane but it includes a change into an equivalent {110} plane. Figure 4 shows snapshots from a movie obtained by MD simulations. The two migration paths were also investigated by the nudged elastic band method. Figure 5(a) depicts the potential energy along the first path at $T=0$ K. The initial and the final states correspond to an extended ⟨110⟩ dumbbell, whereas the ⟨110⟩ dumbbell forms the intermediate state. Figure 5(b) shows schematically the exchange of atoms during the transformation between these configurations. For the second migration path two additional intermediate states were found [Fig. 6(a)], but they are very similar to the ⟨110⟩ dumbbell. The exchange of atoms along the second path is illustrated in Fig. 6(b). Figures 5(a) and 6(a) demonstrate that at $T=0$ K the barriers of the first and the second migration paths are nearly identical. Similarly to the case of vacancy migration these barriers are somewhat higher than the effective barrier obtained by MD simulations (Table II), due to the fact that the latter includes entropy contributions. It should be noted that the first migration path was also observed by Kakimoto *et al.*[37] and Nastar *et al.*[42] using the SW potential. Hane *et al.*[35] who also used the SW potential as well as Nastar *et al.*[42] found migration paths that include a rotation of the ⟨110⟩ dumbbell. However, these paths are not identical to the second path described above.

The previous discussion shows that in the case of the SW potential the self-interstitial migrates mainly via two dumbbell configurations, i.e., the migration of atoms is dominated by a dumbbell mechanism. On the other hand the statistical diffusion theory of Compaan and Haven[16] assumes the interstitialcy mechanism where the self-interstitial configuration moves from one distinctive interstitial site to another by the exchange ("kickout") between the atom on the interstitial site and the nearby lattice atom. As shown schematically in a two-dimensional plot (Fig. 7) the kickout of a lattice atom by a "marked" or "tracer" atom on an interstitial site is not correlated with the previous kickout of the tracer atom, whereas the subsequent kickout of the tracer atom is correlated with the kickout performed by the tracer atom before. Conversely, in the case of a dumbbell mechanism it is not possible to find consecutive atomic jumps that are not corre-

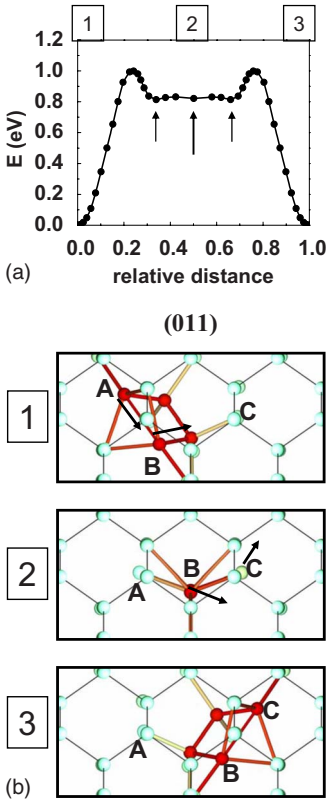

FIG. 6. (Color online) The second migration path of the self-interstitial (cf. Fig. 4) studied by the nudged elastic band method: (a) depicts the potential energy along the path from the extended ⟨110⟩ dumbbell to the ⟨110⟩ dumbbell and vice versa. The long arrow denotes the state of the ⟨110⟩ dumbbell, whereas the short arrows show two intermediate states which are very similar to the ⟨110⟩ dumbbell. The exchange of atoms during the transformation between the different dumbbell configurations is illustrated in (b).

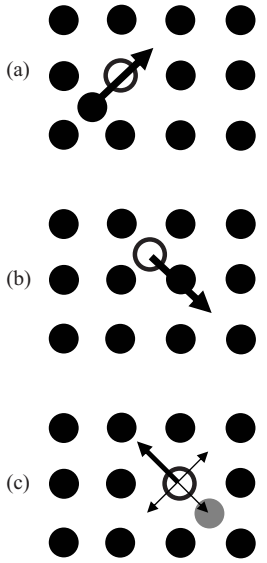

FIG. 7. Illustration of the interstitialcy mechanism in a two-dimensional cubic lattice [cf. Manning (Ref. 43)]: the kickout of a lattice atom (filled circle) by a tracer atom (open circle) at an interstitial site (b) is not correlated with the previous kickout of the tracer atom from a lattice site (a). However, the subsequent kickout of the tracer atom (c) is correlated with the kickout performed by the tracer atom before (b) since it has a greater than random probability on its next jump of jumping back to its previous interstitial site (thick arrow). This is due to the fact that there is a greater than random probability that the (gray) lattice atom stays on the interstitial site until the next jump of the tracer atom takes place. Therefore, a jump of the tracer atom in another direction (thin arrows) which may occur when an interstitial approaches the tracer atom from another side is less probable. In other words, the correlation occurs because it is more probable that the tracer atom is kicked out by the (gray) interstitial and moves back to its original position than that the (gray) atom moves away and another atom arrives as an interstitial in the immediate neighborhood of the tracer.

lated. Therefore, the diffusion-correlation factor f_I=0.59 obtained by present MD simulations using the SW potential (Table II) does not agree with the value 0.73 determined by the statistical diffusion theory assuming the interstitialcy mechanism.[16]

MD simulations using the T3 potential yield a value for the diffusion-correlation factor which is very close to that determined by Compaan and Haven[16] (Table II). The small deviation should be due to statistical errors in the calculation of the diffusion coefficients. The analysis of the atomic migration processes demonstrates that the interstitialcy mechanism prevails. In the temperature range investigated two main migration paths are observed. The first path (Fig. 8) consists of the transformation from the tetrahedral self-interstitial to the ⟨110⟩ dumbbell and vice versa. The atom on the tetrahedral interstitial site "kicks out" an adjacent lattice atom to another tetrahedral interstitial position. During this process the self-interstitial configuration moves in a {110} plane and into a ⟨110⟩ direction. The same migration path was already found by Marques *et al.*[33] who also used the T3 potential in their MD simulations of self-interstitial migration. The second migration path is characterized by the transformation from the tetrahedral self-interstitial to the ⟨100⟩ dumbbell and vice versa. Figure 9 illustrates that the atom at the tetrahedral interstitial position interacts with a nearby lattice atom and forms the ⟨100⟩ dumbbell. Afterward, the former lattice atom is kicked out and moves to another tetrahedral interstitial position. The motion of the self-interstitial configuration takes places in a {110} plane and is directed into a ⟨100⟩ direction.

The diffusion-correlation factor calculated in the present work can be only compared with the value f_I=0.75 given by MD simulations based on the density-functional theory[40,41] since in other previous papers either the self-interstitial diffusivity D_I or the self-diffusion coefficient per self-interstitial D_s^I were determined. Although this value is very close to the result determined by assuming the interstitialcy mechanism,[16] the analysis of self-interstitial migration performed in Refs. 40 and 41 clearly shows that other mechanisms dominate, among them the transition between the simple and the extended ⟨110⟩ dumbbell. The mechanism observed in tight-binding MD simulations of Tang *et al.*[38] and Roberts *et al.*[39] is similar to the first migration path obtained in present investigations using the T3 potential, namely, the transformation from the tetrahedral self-interstitial to the ⟨110⟩ dumbbell and vice versa.

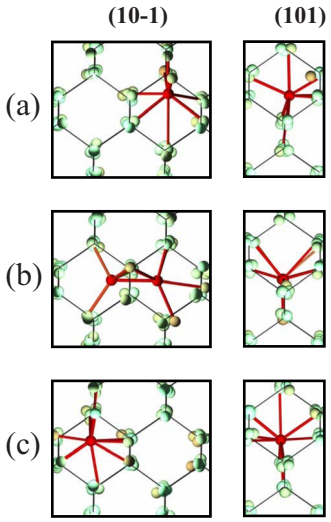

FIG. 8. (Color online) Snapshots from a typical movie obtained from MD simulations of self-interstitial migration using the Tersoff potential (Ref. 20). The figures depict the first migration path which consists of the transformation from (a) the tetrahedral self-interstitial to (b) the ⟨110⟩ dumbbell and (c) vice versa. The atom on the tetrahedral interstitial site kicks out an adjacent lattice atom which moves to another tetrahedral interstitial position. During this process the self-interstitial configuration moves in a {110} plane and into a ⟨110⟩ direction.

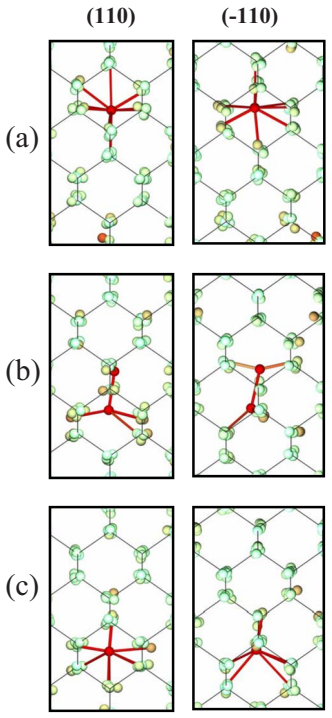

FIG. 9. (Color online) Snapshots from a movie obtained from MD simulations of self-interstitial migration using the Tersoff potential (Ref. 20). The figures illustrate the second migration path which is characterized by the transformation from the tetrahedral self-interstitial to the ⟨110⟩ dumbbell and vice versa. The atom at the tetrahedral interstitial position interacts with a neighboring lattice atom and forms the ⟨110⟩ dumbbell. Then the former lattice atom is kicked out and jumps to another tetrahedral interstitial position. The motion of the self-interstitial configuration occurs in a {110} plane and is directed into a ⟨100⟩ direction.

It was mentioned above that in the case of the T3 potential the effective migration barrier of the vacancy may increase at temperatures below the range studied by the present MD simulations. A similar behavior is also observed for the self-interstitial migration.[30]

IV. CONCLUSIONS

Vacancy and self-interstitial migration as well as the corresponding mobility of silicon atoms have been investigated by comprehensive classical MD simulations using the SW and the T3 potentials. The simulations have been performed in the temperature range between 800 and 1600 K and over 5–1200 ns. In contrast to most of the previous studies both the point defect diffusivity and the self-diffusion coefficient per defect have been calculated separately so that the diffusion-correlation factor can be determined. In the temperature range considered, the diffusion-correlation factors f_V and f_I are constant since the effective migration barriers in the exponents of the corresponding self-diffusion coefficients per defect and defect diffusivities are nearly identical. Simulations with the SW potential as well with the T3 potential show that vacancy migration consists in the transformation of the tetrahedral vacancy to the split vacancy and vice versa. This simple mechanism was also assumed in the statistical diffusion theory of Compaan and Haven.[15] Therefore, the value of the diffusion-correlation factor f_V obtained in the present work is rather similar to that derived by these authors. Self-interstitial diffusion is more complex. The migration mechanisms found by MD simulations using the T3 potential are different to those obtained by the SW potential. In the former case the interstitialcy mechanism prevails, where an interstitial configuration moves from one distinctive interstitial site to another by the kickout of a nearby lattice atom. Therefore, the value of the diffusion-correlation factor f_I calculated in this work is nearly equal to that determined by the statistical diffusion theory which assumes the interstitialcy mechanism.[16] Two main migration mechanisms have been found: (i) the transformation of the tetrahedral interstitial to the ⟨110⟩ dumbbell and vice versa and (ii) the transformation of the tetrahedral interstitial to the ⟨100⟩ dumbbell and vice versa. In the case of the SW potential self-interstitial migration is dominated by a dumbbell mechanism. In contrast to the interstitialcy mechanism it is not possible to find consecutive atomic jumps that are not correlated. Therefore, the diffusion-correlation factor f_I obtained by present MD simulations does not agree with the value determined by the statistical diffusion theory.[16] The dominating migration mechanism is the transformation between the extended ⟨110⟩ dumbbell and the ⟨110⟩ dumbbell and vice versa. This process occurs either in a single {110} plane or includes a change into an equivalent {110} plane.

As mentioned in Sec. I, results of recent investigations on intrinsic point defects in silicon using a unified view from crystal growth, wafer processing, metal diffusion,[17] and on simultaneous self-diffusion and dopant diffusion in isotope

heterostructures[10] demonstrate that in the framework of state-of-the-art modeling the best interpretation of experimental data can be given by assuming $f_I \approx 0.6$. This corresponds to the value obtained by the present atomistic study using the SW potential. Therefore, the self-interstitial migration in Si should mainly occur via a dumbbell mechanism.

ACKNOWLEDGMENTS

F. Gao was supported by the Division of Materials Science and Engineering, Office of Basic Energy Sciences, U.S. Department of Energy under Contract No. DE-AC05-76RL01830.

*Corresponding author. FAX: +49 351 260 3285; m.posselt@fzd.de

[1] K. C. Pandey, Phys. Rev. Lett. **57**, 2287 (1986).
[2] H. Bracht, N. A. Stolwijk, and H. Mehrer, Phys. Rev. B **52**, 16542 (1995).
[3] H. Bracht, E. E. Haller, and R. Clark-Phelps, Phys. Rev. Lett. **81**, 393 (1998).
[4] H. Bracht, Proc.-Electrochem. Soc. **99-1**, 357 (1999).
[5] A. Ural, P. B. Griffin, and J. D. Plummer, Phys. Rev. Lett. **83**, 3454 (1999).
[6] P. E. Blöchl, E. Smargiassi, R. Car, D. B. Laks, W. Andreoni, and S. T. Pantelides, Phys. Rev. Lett. **70**, 2435 (1993).
[7] Y. Shimizu, M. Uematsu, and K. M. Itoh, Phys. Rev. Lett. **98**, 095901 (2007).
[8] M. Posselt, F. Gao, and D. Zwicker, Phys. Rev. B **71**, 245202 (2005).
[9] H. Bracht, Nucl. Instrum. Methods Phys. Res. B **253**, 105 (2006).
[10] H. Bracht, H. H. Silvestri, I. D. Sharp, and E. E. Haller, Phys. Rev. B **75**, 035211 (2007).
[11] N. A. Stolwijk, B. Schuster, and J. Hölzl, Appl. Phys. A: Solids Surf. **A33**, 133 (1984).
[12] N. A. Stolwijk, J. Hölzl, W. Frank, E. R. Weber, and H. Mehrer, Appl. Phys. A: Solids Surf. **A39**, 37 (1986).
[13] A. Giese, H. Bracht, N. A. Stolwijk, and D. Baither, Mater. Sci. Eng., B **71**, 160 (2000).
[14] A. Ural, P. B. Griffin, and J. D. Plummer, J. Appl. Phys. **85**, 6440 (1999).
[15] K. Compaan and Y. Haven, Trans. Faraday Soc. **52**, 786 (1956).
[16] K. Compaan and Y. Haven, Trans. Faraday Soc. **54**, 1498 (1958).
[17] V. V. Voronkov and R. Falster, Solid State Phenom. **108-109**, 1 (2005).
[18] H. Bracht, Physica B (Amsterdam) **376-377**, 11 (2006).
[19] F. H. Stillinger and T. A. Weber, Phys. Rev. B **31**, 5262 (1985).
[20] J. Tersoff, Phys. Rev. B **38**, 9902 (1988).
[21] H. Balamane, T. Halicioglu, and W. A. Tiller, Phys. Rev. B **46**, 2250 (1992).
[22] H. J. C. Berendsen, J. P. M. Postma, W. F. van Gunsteren, A. DiNola, and J. R. Haak, J. Chem. Phys. **81**, 3684 (1984).
[23] G. H. Gilmer, T. Diaz de la Rubia, D. M. Stock, and M. Jaraiz, Nucl. Instrum. Methods Phys. Res. B **102**, 247 (1995).
[24] Yu. N. Osetsky, Defect Diffus. Forum **188-190**, 71 (2001).
[25] J. Marian, B. D. Wirth, A. Caro, B. Sadigh, G. R. Odette, J. M. Perlado, and T. Diaz de la Rubia, Phys. Rev. B **65**, 144102 (2002).
[26] M. W. Guinan, R. N. Stuart, and R. J. Borg, Phys. Rev. B **15**, 699 (1977).
[27] H. Jonsson, G. Mills, and K. W. Jacobsen, in *Classical and Quantum Dynamics in Condensed Phase Simulations*, edited by B. J. Berne, G. Ciccotti, and D. F. Coker (World Scientific, Singapore, 1998), p. 385.
[28] G. Henkelman and H. Jonsson, J. Chem. Phys. **113**, 9978 (2000).
[29] P. J. Ungar, T. Takai, T. Halicioglu, and W. A. Tiller, J. Vac. Sci. Technol. A **11**, 224 (1993).
[30] P. J. Ungar, T. Halicioglu, and W. A. Tiller, Phys. Rev. B **50**, 7344 (1994).
[31] H. R. Schober, Phys. Rev. B **39**, 13013 (1989).
[32] K. Nishihira and T. Motooka, Phys. Rev. B **66**, 233310 (2002).
[33] L. A. Marques, L. Pelaz, P. Castrillo, and J. Barbolla, Phys. Rev. B **71**, 085204 (2005).
[34] P. Erhart and K. Albe, Phys. Rev. B **71**, 035211 (2005).
[35] M. Hane, T. Ikezawa, and A. Furukawa, IEICE Trans. Electron. **83-C**, 1247 (2000).
[36] T. Sinno, Z. K. Jiang, and R. A. Brown, Appl. Phys. Lett. **68**, 3028 (1996).
[37] K. Kakimoto, T. Umehara, and H. Ozoe, J. Cryst. Growth **210**, 54 (2000).
[38] M. Tang, L. Colombo, J. Zhu, and T. Diaz de la Rubia, Phys. Rev. B **55**, 14279 (1997).
[39] B. W. Roberts, W. Luo, K. A. Johnson, and P. Clancy, Chem. Eng. J. **74**, 67 (1999).
[40] B. Sahli, in *Ab-initio Molecular Dynamics Simulation of Diffusion in Silicon*, Series in Microelectronics Vol. 181, edited by W. Fichtner, Q. Huang, H. Jäckel, H. Melchior, G. S. Moschytz, and G. Tröster (Hartung-Gorre Verlag, Konstanz, 2007).
[41] B. Sahli and W. Fichtner, Phys. Rev. B **72**, 245210 (2005).
[42] M. Nastar, V. V. Bulatov, and S. Yip, Phys. Rev. B **53**, 13521 (1996).
[43] J. R. Manning, *Diffusion Kinetics for Atoms in Crystals* (Van Nostrand, Princeton, 1968).